INTERNATIONAL JOURNAL FOR NUMERICAL METHODS IN FLUIDS
Int. J. Numer. Meth. Fluids **28**: 381–394 (1998)

NUMERICAL SOLUTION OF A TWO-DIMENSIONAL FLUIDIZED BED MODEL

I. CHRISTIE*, G.H. GANSER AND J.W. WILDER

Department of Mathematics, West Virginia University, PO Box 6310, Morgantown, WV 26506, USA

SUMMARY

The numerical solution of a model describing a two-dimensional fluidized bed is considered. The model takes the form of a hyperbolic system of conservation laws with source term, coupled with an elliptic equation for determining a streamfunction. Operator splitting is used to produce homogeneous one-dimensional hyperbolic systems and ordinary differential equations involving the source term. The one-dimensional hyperbolic problems are solved using Roe's method with the addition of an entropy fix. The numerical procedure is second-order in time and first-order in space. Second-order-accuracy in space is obtained using flux limiting techniques. Numerical experiments which show the development of bubbles in the bed are presented. The familiar kidney-shaped bubble, observed experimentally, is found when using the method which is second-order in space. On the same mesh, the first-order method produces bubbles which are no longer kidney-shaped. © 1998 John Wiley & Sons, Ltd.

KEY WORDS: fluidized bed; hyperbolic PDEs; Roe's method

1. INTRODUCTION

In a fluidized bed, particles confined to a vertical column are suspended by a sufficiently strong upward volumetric flux of fluid. In some circumstances the fluid flows uniformly through a bed of particles of constant concentration. A more interesting and difficult situation, however, is when the fluidized bed exhibits a phenomenon known as slugging or bubbling, where regions of low particle concentrations propagate up the bed.

In this paper, a fluidized bed model is solved numerically in two space dimensions. The model, which does not contain particle viscosity, consists of a hyperbolic system of conservation laws with a source term and a coupled elliptic equation for determining a streamfunction. The origins of the model can be found in the review article by Drew [1], where a general set of equations modelling dispersed two-phase flow is derived by averaging the microscopic equations of motion, leading to a continuum model for both phases. In the present study, heavy particles are dispersed in a gas and gas inertia is neglected, thereby reducing the conservation of momentum equation for the gas phase to Darcy's law. Many papers on this subject have used this type of model, where the particle phase is modelled as a Newtonian fluid with a particle phase viscosity (which is much larger in magnitude than the fluid viscosity). However, as in single phase flow, the question arises as to the possibility of ignoring particle phase viscosity in certain circumstances and studying the inviscid equations. In the current

* Correspondence to: Department of Mathematics, West Virginia University, PO Box 6310, Morgantown, WV 26506, USA. Tel: +1 304 2932011, Ext: 2320; Fax: +1 304 2933982; E-mail: ichristi@wvnvm.wvnet.edu

CCC 0271–2091/98/130381–14$17.50

Received February 1997
Accepted October 1997

model, this results in a problem with real characteristics, as opposed to the more difficult case of complex characteristics, in more general two-phase flows [2].

By studying one-dimensional travelling wave solutions with variations in only the vertical direction, some authors [3,4] have concluded that particle viscosity, no matter how small, is responsible for the oscillations or slug-like structure of these solutions. However, Ganser and Lightbourne [5] have shown mathematically for a model without particle viscosity, that there exist one-dimensional solutions which possess the oscillatory and slug-like behaviour. One-dimensional numerical simulations by Christie *et al.* [6] also indicate that the model without particle viscosity exhibits slugging.

Although experimental work has demonstrated that one-dimensional slugging does occur, solutions with variations in the horizontal direction as well as the vertical direction are much more typical. The focus of this paper is to numerically determine solutions with variations in the vertical and horizontal directions. In particular, the response of an already fluidized bed to additional gas blown through a centrally located orifice at the bottom of the bed is studied.

The numerical scheme is an extension of that developed by Christie *et al.* [6], for the one-dimensional case. The well-known splitting technique of Strang [7] is used to reduce the two-dimensional model equations to a sequence of problems involving ordinary differential equations, hyperbolic systems in one space dimension, and an elliptic equation for the streamfunction. Roe's method [8] with a superbee flux limiter, and the entropy fix of Harten and Hyman [9] are applied to the split hyperbolic system. A second-order finite difference method is used to solve the elliptic equation and the ordinary differential equations produced by the splitting are solved in closed form. The resulting method has second-order accuracy in space and time and is explicit in time.

Roe's method uses an approximate Riemann solver on the hyperbolic systems. Exact Riemann solvers are also available and were applied to a one-dimensional hyperbolic fluidized bed model by Christie and Palencia [10]. Both papers [6,10] contain results which demonstrate one-dimensional slugging.

Other work on numerical solutions of two-dimensional fluidized bed models includes the paper by Pritchett *et al.* [11], where the model includes a particle viscosity term in the momentum equations and is solved by an implicit finite difference scheme. Syamlal [12] and Syamlal and O'Brien [13] solve a hyperbolic system using an implicit, first-order in space, donor-cell approach and report a smoothing of discontinuities. In some papers, a line of symmetry is used in the calculations so that the numerical results display perfect symmetry. In this paper a forced symmetric solution has been avoided.

In the next section, a two-dimensional mathematical model of a fluidized bed is described. Later, Roe's method for the operator split system is presented. A first-order scheme in space is derived and, using flux limiters, a second-order scheme in space is obtained. Numerical results show the evolution of bubbles. The familiar kidney-shaped bubble is found with the second-order method but is not present in the results obtained when using the first-order method on the same mesh.

2. MATHEMATICAL MODEL

A continuum approach is used for both the particle phase and the gas phase. The equations are given by

$$\frac{\partial \alpha}{\partial t} + \nabla \cdot (\alpha v_p) = 0, \tag{1}$$

$$\frac{\partial (1-\alpha)}{\partial t} + \nabla \cdot (1-\alpha) v_g = 0, \tag{2}$$

$$\frac{\partial (\rho_p \alpha v_p)}{\partial t} + \nabla \cdot (\alpha \rho_p v_p v_p) = -\alpha \nabla p_g - \nabla \alpha (p_p - p_g) - \rho_p \alpha g \hat{z} + B(\alpha)(v_g - v_p), \tag{3}$$

$$0 = -(1-\alpha)\nabla p_g - B(v_g - v_p). \tag{4}$$

Equations (1) and (2) are the continuity equations for each phase and (3) and (4) are the momentum balances. The particle volume concentration is denoted by α, v_p, v_g are the velocity vectors of the particle and gas phases, ρ_p, ρ_g are the actual densities of the particles and gas, p_p, p_g are the pressures, g is the acceleration due to gravity, $\hat{z}$ is a unit vector in the z-direction, and $B(\alpha)$ is the drag coefficient. Since $\rho_p \gg \rho_g$, the inertia of the gas has been neglected in Equation (4), leaving Darcy's law.

As in Needham and Merkin [4], Fanucci *et al.* [3,14], and Liu [15,16], a linear drag law is used here, primarily because of its simplicity. The difference between the pressures in the two phases is modelled as

$$\alpha(p_p - p_g) = \rho_p v_t^2 F(\alpha), \tag{5}$$

where v_t is the terminal velocity of an isolated particle. It is usually assumed that $F'(\alpha) > 0$. For example, in Needham and Merkin [4], Liu [15,16], and Homsy *et al.* [17], F' is assumed to be a positive constant, and in Fanucci *et al.* [3,14], F' exhibits rapid growth for larger particle concentrations. In this last choice for F', the physically motivated properties are that F' is small for small α and becomes infinite as α approaches a packing concentration $\alpha_p < 1$. These are essentially the properties of an incompressible model. A form for $F'(\alpha)$ that captures these more realistic features is

$$v_t^2 F'(\alpha) = \frac{s^2 \alpha^2}{(\alpha_p - \alpha)^2}. \tag{6}$$

The constant s can be related to the linear stability of the equilibrium solutions that correspond to the states of uniform fluidization. For a constant particle concentration of $\alpha = \alpha_0$ ($0 \le \alpha_0 \le \alpha_p$), there is a solution of the system of Equations (1)–(4) with $v_p = 0$ when the flux of vertical gas, j, entering the bed satisfies

$$j = \frac{\alpha_0 \rho_p g (1-\alpha_0)^2}{B(\alpha_0)}. \tag{7}$$

The kinematic wave speed associated with this equilibrium solution is

$$c_k(\alpha_0) = \frac{\mathrm{d}}{\mathrm{d}\alpha}\left(\alpha j - \frac{\alpha^2 \rho g (1-\alpha)^2}{B(\alpha)} \right)\Bigg|_{\alpha = \alpha_0}. \tag{8}$$

When the higher order speed $v_t\sqrt{F'(\alpha_0)}$ satisfies

$$v_t \sqrt{F'(\alpha_0)} > c_k(\alpha_0), \tag{9}$$

the bed is linearly stable to perturbations in the vertical direction. The state $\alpha = \alpha_{0u}$ is the critical state that divides linearly stable and unstable solutions and is defined by

$$v_t \sqrt{F'(\alpha_{0u})} = c_k(\alpha_{0u}). \tag{10}$$

Once α_{0u} is chosen, this equation determines s. As $\alpha_{0u} \to \alpha_p$, $s \to 0$ and Equation (6) approaches the incompressible model.

The continuity equations are manipulated in the following manner. Adding Equations (1) and (2) implies that the vector field $\alpha v_p + (1-\alpha)v_g$ is divergence-free. At most, problems with spatial variations in the vertical direction (z-axis) and the horizontal direction (x-axis) will be studied, therefore, this constraint on $\alpha v_p + (1-\alpha)v_g$ can be satisfied by the introduction of a streamfunction $\psi(x, z, t)$ with the properties

$$\alpha v_{px} + (1-\alpha)v_{gx} = \frac{\partial \psi}{\partial z}, \tag{11}$$

$$\alpha v_{pz} + (1-\alpha)v_{gz} = -\frac{\partial \psi}{\partial x}. \tag{12}$$

The subscripts x and z denote the first and second components of the velocity vectors, respectively. Equations (11) and (12) can then be used to eliminate v_{gx} and v_{gz} from the problem.

The normalized equations used in the numerical analysis have v_t as the velocity scale, v_t^2/g and v_t/g as the length and time scales, respectively. As can be seen from Equations (11) and (12), the scale for the streamfunction is v_t^3/g. For simplicity, the notation for the scaled streamfunction will remain as ψ. The drag coefficient as it appears in Equation (4) is given by

$$B(\alpha) = \frac{\alpha \rho_p g (1-\alpha)^{2-N}}{v_t}. \tag{13}$$

Typically, the real number N is chosen according to $2 \le N \le 4$ [4,17] and in this numerical calculation, $N = 3.5$ is selected. After normalization, the drag coefficient becomes simply $\alpha(1-\alpha)^{2-N}$ and will continue to be denoted by $B(\alpha)$ for simplicity.

The normalized two-dimensional equations consist of a hyperbolic system

$$\frac{\partial \alpha}{\partial t} + \frac{\partial m}{\partial x} + \frac{\partial n}{\partial z} = 0, \tag{14}$$

$$\frac{\partial m}{\partial t} + \frac{\partial (mu + F(\alpha))}{\partial x} + \frac{\partial (nu)}{\partial z} = \frac{B(\alpha)}{(1-\alpha)^2}\left(\frac{\partial \psi}{\partial z} - u\right), \tag{15}$$

$$\frac{\partial n}{\partial t} + \frac{\partial (mv)}{\partial x} + \frac{\partial (nv + F(\alpha))}{\partial z} = \frac{B(\alpha)}{(1-\alpha)^2}\left(-\frac{\partial \psi}{\partial x} - v\right) - \alpha, \tag{16}$$

with $m(x, z, t)$ denoting the horizontal momentum, and $n(x, z, t)$ the vertical momentum. The horizontal velocity $u(x, z, t)$ and the vertical velocity $v(x, z, t)$ are defined by $m = \alpha u$ and $n = \alpha v$. The streamfunction $\psi(x, z, t)$, which corresponds to the total volumetric flux [18], is obtained by solving the elliptic equation

$$\frac{\partial}{\partial x}\left(\left(\alpha \frac{\partial \psi}{\partial x} + n\right)(1-\alpha)^{-N}\right) + \frac{\partial}{\partial z}\left(\left(\alpha \frac{\partial \psi}{\partial z} - m\right)(1-\alpha)^{-N}\right) = 0. \tag{17}$$

The spatial domain of the system (14)–(17) is a rectangle with $-x_R \le x \le x_R$ and $-z_R \le z \le z_R$. In the numerical calculations, initial conditions will be specified for α, m, n, and then Equation (17) will be solved for ψ. The boundary conditions are given by

$$u = 0 \text{ at } x = -x_R, x_R, \text{ and } z_R, \tag{18}$$

$$v = 0 \text{ at } z = -z_R. \tag{19}$$

The case of a centrally located ($x=0$, $z=-z_{\mathrm{R}}$) jet of gas of width $2x_b$ ($-x_b<x<x_b$ inside the jet) is considered. The background fluidizing gas entering at the bottom of the bed is $j_M=(1-\alpha_M)^N$ where α_M is chosen between α_{p} and α_{0u}. Initially, the flux of gas entering at the bottom of the bed inside the jet is increased to $j>j_M$. At the top of the bed the total volumetric flux that entered at $z=-z_{\mathrm{R}}$, given by $x_b(j-j_M)/x_{\mathrm{R}}+j_M$, is assumed to be evenly dispersed. The boundary conditions for ψ are

$$\psi(-x_{\mathrm{R}}, z, t)=0, \tag{20}$$

$$\psi(x_{\mathrm{R}}, z, t)=-2x_{\mathrm{R}}j_M+2x_b(j_M-j), \tag{21}$$

$$\psi(x, -z_{\mathrm{R}}, t)=\left\{\begin{array}{ll} -j_M(x+x_{\mathrm{R}}) & -x_{\mathrm{R}}\le x\le -x_b \\ -j(x+x_b)-j_M(x_{\mathrm{R}}-x_b) & -x_b<x<x_b \\ -j_M(x+x_{\mathrm{R}})+2x_b(j_M-j) & x_b\le x\le x_{\mathrm{R}} \end{array}\right\}, \tag{22}$$

$$\psi(x, z_{\mathrm{R}}, t)=(-j_M+x_b(j_M-j)/x_{\mathrm{R}})(x+x_{\mathrm{R}}). \tag{23}$$

3. NUMERICAL METHOD

To determine the behaviour of the solutions of Equations (14)–(17), an extension of the method developed by Christie *et al.* [6], for a related one-dimensional problem is considered. To describe the numerical method, write the system (14)–(17) in the form

$$w_t+f(w)_x+g(w)_z=b, \tag{24}$$

where

$$w=[\alpha, m, n]^T,$$

$$f(w)=[m, mu+F(\alpha), mv]^T,$$

$$g(w)=[n, nu, nv+F(\alpha)]^T,$$

$$b=\left[0, \frac{B(\alpha)}{(1-\alpha)^2}\left(\frac{\partial\psi}{\partial z}-u\right), \frac{B(\alpha)}{(1-\alpha)^2}\left(-\frac{\partial\psi}{\partial x}-v\right)-\alpha\right]^T,$$

and subscripts denote partial derivatives. The numerical method makes use of the non-conservation form of Equation (24) which, from differentiation of $f(w)$ and $g(w)$, is given by

$$w_t+J(w)w_x+K(w)w_z=b. \tag{25}$$

The Jacobian matrices are

$$J=\left(\begin{array}{ccc} 0 & 1 & 0 \\ -\lambda_+\lambda_- & \lambda_++\lambda_- & 0 \\ -\lambda\mu & \mu & \lambda \end{array}\right), \tag{26}$$

and

$$K=\left(\begin{array}{ccc} 0 & 0 & 1 \\ -\lambda\mu & \mu & \lambda \\ -\mu_+\mu_- & 0 & \mu_++\mu_- \end{array}\right), \tag{27}$$

where $\lambda = u$, $\lambda_{\pm} = u \pm \sqrt{F'}$ are the eigenvalues of J and $\mu = v$, $\mu_{\pm} = v \pm \sqrt{F'}$ are the eigenvalues of K.

To advance the solution of Equation (24) over one time step Δt, the splitting due to Strang [7] produces the following sequence of problems to be solved at each time level:

$$w_t = b, \tag{28}$$

$$w_t + J(w)w_x = 0, \tag{29}$$

$$w_t + K(w)w_z = 0, \tag{30}$$

$$w_t + J(w)w_x = 0, \tag{31}$$

$$w_t = b. \tag{32}$$

The starting values for each equation (29)–(32) are provided by the solution of the preceding equation. For Equation (28) the starting values are obtained from the solution of Equation (32) computed at the previous time step (except at $t = 0$ when the initial data are used). Equation (30) is solved with a time step of Δt and the other four equations are each solved with a time step of $\Delta t/2$. The scheme has second-order-accuracy in time.

The streamfunction ψ appears in terms of its first partial derivatives only in Equations (28) and (32). Therefore, Equation (17) is solved initially and then immediately before and after solving Equation (32) at each time step. Equation (17) is discretized using central differences and the resulting system of algebraic equations is solved by Gauss–Seidel iteration. The derivatives of ψ required in Equations (28) and (32) are then approximated using central differences.

If it is assumed that the first partial derivatives of the streamfunction remain constant across the fractional step then Equations (28) and (32) can be solved in closed form. Their solutions are

$$\alpha = \alpha^*, \tag{33}$$

$$m = \alpha^* \frac{\partial \psi}{\partial z}(1 - E) + m^* E, \tag{34}$$

$$n = \alpha^*(1 - \alpha^*)^N \left(1 + (1 - \alpha^*)^{-N} \frac{\partial \psi}{\partial x}\right)(E - 1) + En^*, \tag{35}$$

where * signifies the starting value for the step and

$$E = \exp(-(1 - \alpha^*)^{-N} \Delta t/2). \tag{36}$$

Equations (29)–(31) are solved using Roe's method. Consider a Riemann problem in which the initial data for each of Equations (29)–(31) are given by the left and right states $w_{\mathrm{L}} = [\alpha_{\mathrm{L}}, m_{\mathrm{L}}, n_{\mathrm{L}}]^T$ and $w_{\mathrm{R}} = [\alpha_{\mathrm{R}}, m_{\mathrm{R}}, n_{\mathrm{R}}]^T$, respectively. The left and right horizontal and vertical velocities can be computed from the formulas $u = m/\alpha$ and $v = n/\alpha$ respectively, if $\alpha \neq 0$.

Roe's method replaces Equations (29) and (31) by the linearized equation

$$w_t + \bar{J}(w_{\mathrm{L}}, w_{\mathrm{R}})w_x = 0, \tag{37}$$

and Equation (30) by

$$w_t + \bar{K}(w_{\mathrm{L}}, w_{\mathrm{R}})w_z = 0, \tag{38}$$

respectively. The approximate Jacobians $\bar{J}$ and $\bar{K}$ satisfy

$$\bar{J}(w_R - w_L) = f(w_R) - f(w_L), \tag{39}$$

$$\bar{K}(w_R - w_L) = g(w_R) - g(w_L), \tag{40}$$

and are not uniquely determined. The following were chosen:

$$\bar{J} = \begin{pmatrix} 0 & 1 & 0 \\ -\bar{\lambda}_+\bar{\lambda}_- & \bar{\lambda}_+ + \bar{\lambda}_- & 0 \\ -\bar{\lambda}\bar{\mu} & \bar{\mu} & \bar{\lambda} \end{pmatrix}, \tag{41}$$

and

$$\bar{K} = \begin{pmatrix} 0 & 0 & 1 \\ -\bar{\lambda}\bar{\mu} & \bar{\mu} & \bar{\lambda} \\ -\bar{\mu}_+\bar{\mu}_- & 0 & \bar{\mu}_+ + \bar{\mu}_- \end{pmatrix}, \tag{42}$$

where $\bar{\lambda} = \bar{u}$, $\bar{\lambda}_\pm = \bar{u} \pm \bar{c}$, $\bar{\mu} = \bar{v}$, and $\bar{\mu}_\pm = \bar{v} \pm \bar{c}$. The averaged velocities are taken as in Roe [8] and Glaister [19] to be

$$\bar{u} = \frac{\sqrt{\alpha_R u_R} + \sqrt{\alpha_L u_L}}{\sqrt{\alpha_R} + \sqrt{\alpha_L}} \quad \text{and} \quad \bar{v} = \frac{\sqrt{\alpha_R v_R} + \sqrt{\alpha_L v_L}}{\sqrt{\alpha_R} + \sqrt{\alpha_L}}. \tag{43}$$

The averaged speed is given by

$$\bar{c}^2 = \frac{(F(\alpha_R) - F(\alpha_L))}{(\alpha_R - \alpha_L)}, \tag{44}$$

or, whenever α_L and α_R are close, by

$$\bar{c}^2 = \frac{dF}{d\alpha}, \quad \text{at } \alpha = \frac{1}{2}(\alpha_R + \alpha_L). \tag{45}$$

The matrices $\bar{J}$ and $\bar{K}$ can be diagonalized because

$$P^{-1}\bar{J}P = \text{diag}(\bar{\lambda}, \bar{\lambda}_-, \bar{\lambda}_+), \tag{46}$$

and

$$Q^{-1}\bar{K}Q = \text{diag}(\bar{\mu}, \bar{\mu}_-, \bar{\mu}_+), \tag{47}$$

where

$$P = \begin{pmatrix} 0 & 1 & 1 \\ 0 & \bar{\lambda}_- & \bar{\lambda}_+ \\ 1 & \bar{\mu} & \bar{\mu} \end{pmatrix} \tag{48}$$

and

$$Q = \begin{pmatrix} 0 & 1 & 1 \\ 1 & \bar{\lambda} & \bar{\lambda} \\ 0 & \bar{\mu}_- & \bar{\mu}_+ \end{pmatrix}. \tag{49}$$

Equations (37) and (38) then uncouple, giving

$$P^{-1}w_t + P^{-1}\bar{J}(w_L, w_R)PP^{-1}w_x = 0, \tag{50}$$

and

$$Q^{-1}w_t + Q^{-1}\bar{K}(w_L, w_R)QQ^{-1}w_z = 0. \tag{51}$$

A discretization of Equations (50) and (51), which has first-order-accuracy in space is now described, and another which has second-order-accuracy.

3.1. First-order method

The spatial domain is subdivided into rectangular cells $[x_{i-1/2}, x_{i+1/2}] \times [z_{j-1/2}, z_{j+1/2}]$, with $x_i = -x_R + (i-1/2)\Delta x$, $z_j = -z_R + (j-1/2)\Delta z$, $i = 1, \ldots, N_x$, $j = 1, \ldots, N_z$, whose sides have the constant lengths $\Delta x = 2x_R/N_x$ and $\Delta z = 2z_R/N_z$. The solution w is assumed to have the constant value $[\alpha_{ij}, m_{ij}, n_{ij}]^T$ in the cell $[x_{i-1/2}, x_{i+1/2}] \times [z_{j-1/2}, z_{j+1/2}]$. Additional, mirror-image cells are included beyond the vertical walls and the bottom of the bed to incorporate the reflecting boundary conditions in Equations (18) and (19).

There are six uncoupled equations in (50) and (51) which are all solved in a similar manner. To illustrate the method, consider the first equation in (50) given by

$$W_t + \bar{\lambda}W_x = 0, \tag{52}$$

where the scalar function W is the first component of the vector $P^{-1}w$. First-order upwind differencing produces

$$W_{ij}^{n+1} = W_{ij}^n - \frac{1}{2}\nu^- \delta_x W_{i+(1/2)j}^n - \frac{1}{2}\nu^+ \delta_x W_{i-(1/2)j}^n, \tag{53}$$

$i = 1, \ldots, N_x$, $j = 1, \ldots, N_z$, $n = 0, \ldots, \Delta t$ is the time step, W_{ij}^n is the numerical approximation to W in cell $[x_{i-1/2}, x_{i+1/2}] \times [z_{j-1/2}, z_{j+1/2}]$ at time $t = t_n$, δ_x is the central difference operator defined by $\delta_x W_{i+(1/2)j}^n = W_{i+1j}^n - W_{ij}^n$, and

$$\nu^{\pm} = (\bar{\lambda} \pm |\bar{\lambda}|)\frac{\Delta t}{\Delta x}. \tag{54}$$

The other components of Equations (50) and (51) are discretized in a similar way.

A modification of the numerical procedure is required to handle the possibility of non-physical shocks which can occur in Roe's method. These were encountered by Christie *et al.* [6] in the one-dimensional problem and avoided by using the entropy fix described by Harten and Hyman [9]. The same technique is used to generate the numerical results presented in this paper.

The time step Δt is chosen to satisfy the CFL condition [20]. The maximum modulus eigenvalue γ of $\bar{J}$ and $\bar{K}$ is computed and the condition

$$\Delta t < \min\{\Delta x, \Delta z\}C/\gamma, \tag{55}$$

where C is a constant between 0 and 1, is checked. The solution is rejected if the condition is violated and the step is repeated, otherwise we proceed to the next time level. In either case, the new time step is chosen as

$$\Delta t < 0.8 \min\{\Delta x, \Delta z\}C/\gamma. \tag{56}$$

The factor 0.8 is included to reduce the number of rejected steps.

3.2. Second-order method

Second-order-accuracy is obtained following the techniques of Roe [21] and Sweby [22]. The first-order scheme (53) is modified by including an antidiffusive flux [22] on the right-hand-side of Equation (53):

$$W_{ij}^{n+1} = W_{ij}^{n} - \frac{1}{2} v^{-} \delta_x W_{i+(1/2)j}^{n} - \frac{1}{2} v^{+} \delta_x W_{i-(1/2)j}^{n} + \mathrm{sgn}(\bar{\lambda})(h_{i+(1/2)j} - h_{i-(1/2)j}), \tag{57}$$

where

$$h_{i+(1/2)j} = -\frac{1}{2}\left(1 - |\bar{\lambda}| \frac{\Delta t}{\Delta x}\right) \bar{\lambda} \frac{\Delta t}{\Delta x} B(\delta_x W_{i+(1/2)j}^{n}, \eta), \tag{58}$$

$$\eta = \delta_x W_{i-(1/2)j}^{n} \quad \text{if} \quad \bar{\lambda} > 0, \tag{59}$$

and

$$\eta = \delta_x W_{i+(3/2)j}^{n} \quad \text{if} \quad \bar{\lambda} < 0, \tag{60}$$

$i = 1, \ldots, N_x$, $j = 1, \ldots, N_z$. The method requires mirror-image cells, in addition to those used in the first-order method, to specify the boundary conditions.

The function $B(\xi, \eta)$ is a flux limiter chosen to maintain monotonicity in the solution. Roe [21] and Sweby [22] describe possible choices of $B(\xi, \eta)$. As in Reference [6] the superbee flux limiter is used here to compute the solution. Christie and Palencia [10] used an alternative flux limiter known as minmod in their method. Defining

$$\mathrm{minmod}(\xi, \eta) = \begin{cases} \xi & \text{if} \quad |\xi| \le |\eta| \\ \eta & \text{if} \quad |\xi| > |\eta| \end{cases}, \tag{61}$$

and maxmod in a similar fashion, the superbee flux limiter is given by

$$B(\xi, \eta) = \begin{cases} \mathrm{maxmod}(\xi, \eta) & \text{if} \quad \dfrac{1}{2} \le \dfrac{\eta}{\xi} \le 2 \\ 2 \ \mathrm{minmod}(\xi, \eta) & \text{if} \quad \dfrac{\eta}{\xi} < \dfrac{1}{2} \quad \text{or} \quad \dfrac{\eta}{\xi} > 2. \\ 0 & \text{if} \quad \xi\eta < 0 \end{cases} \tag{62}$$

The second-order method also includes an entropy fix. The time step selection is identical to that of the first-order method.

4. NUMERICAL RESULTS

A fluidized bed with a total height of 4 units ($z_R = 2$) and total width of 3 units ($x_R = 1.5$) is now considered. Initially, the concentration of particles is $\alpha = \alpha_{0u}$ and the velocities are $u = v = 0$. Equation (17) is solved to find ψ. At time $t > 0$, a jet of gas with a total width of 0.2 units ($x_b = 0.1$), enters from the bottom of the bed, centred at the point $(0, -2)$ in the x–z-plane. The flux of gas in the jet is $j = (1 - \alpha_0)^{3.5}$ with $\alpha_0 = 0.2$. Elsewhere at the bottom of the bed the flux is $j_M = (1 - \alpha_M)^{3.5}$ with $\alpha_M = \alpha_{0u} = 0.57$.

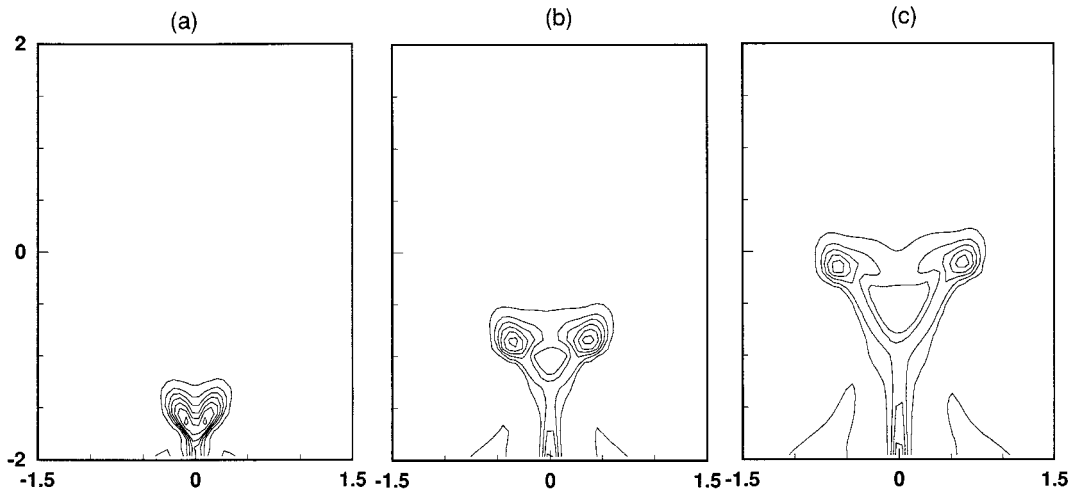

Figure 1. Contour plots of α at $t = 2$, 4 and 6 obtained using the first-order method.

Results for the first-order method are shown in Figure 1. A 101×101 grid ($N_x = N_z = 101$) is used. Contour lines show the particle concentration in increments of 0.05 units with the outermost contour representing a concentration of 0.55. The solution is given at times $t = 2$, 4 and 6 units (Figure 1 (a), (b) and (c) respectively). A bubble develops near the jet and gradually travels up the bed. By a time of $t = 2$, there is an indication that two adjacent bubbles are forming and are travelling up the bed together and by $t = 6$ this is more noticeable.

In Figure 2 the results obtained using the second-order method are shown. Again, a 101×101 grid is used and contour plots denote particle concentration increments of 0.05 units, with 0.55 as the outermost value. Figure 2(a), (b) and (c) show the concentrations at times 2, 4 and 6 respectively. In this case, the more familiar kidney-shaped bubble is present.

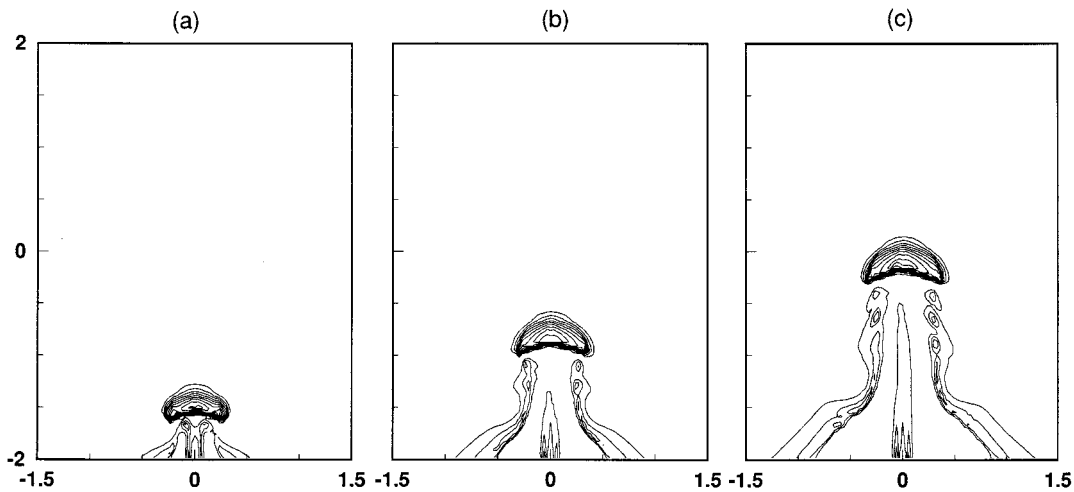

Figure 2. Contour plots of α at $t = 2$, 4 and 6 obtained using the second-order method.

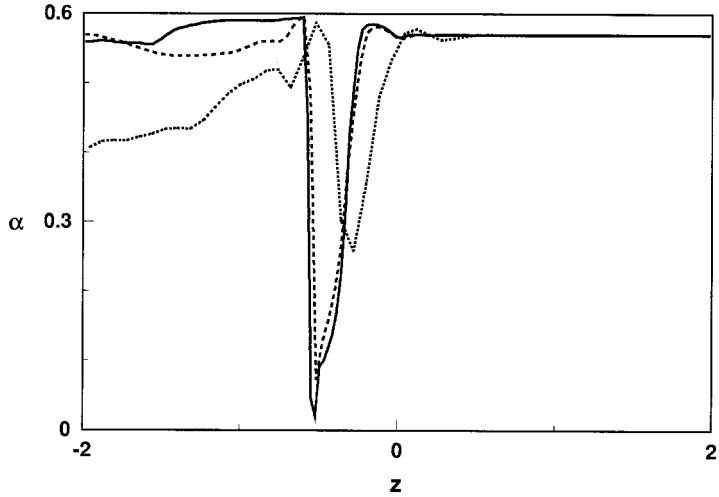

Figure 3. Centre line plots ($x = 0$) of concentration against z at $t = 4$. ($\cdots$) 51×51 grid; (----) 101×101 grid; (—) 151×151 grid.

A much finer grid would be necessary in the first-order method to obtain an accuracy comparable to that of the second-order method. Even on a 151×151 grid the behaviour of the first-order method is similar to that shown in Figure 1. The computational cost of the second-order is higher than for the first-order method on the same grid. However, to achieve comparable accuracy, the first-order method would require such a fine grid that its cost would be much higher than that for the second-order method.

The comparison between the first- and second-order methods given by Figures 1 and 2 is interesting. The second-order method reproduces the kidney-shaped bubble and the first-order method does not. The second-order results are obtained from a process which includes the first-order method as a first-stage at each time step. The results in Figures 1 and 2 are typical of those found with a large range of values of the parameters and they clearly demonstrate the superiority of the second-order method. The remainder of the results presented in the paper were found using the second-order method.

Figure 3 is a graph of the concentration along the centre line $x = 0$ at a time of $t = 4$ and refined mesh. The grid sizes used are 51×51 (small dashes), 101×101 (large dashes) and 151×151 (continuous line). An odd number of points was selected in order to place a node exactly at the middle of the jet. Each curve indicates the existence of a shock immediately below the bubble. The results are reminiscent of the one-dimensional calculations given by Christie *et al.* [6]. For the two finer meshes in Figure 3 the curves are similar, but on the coarse mesh there is a large difference, particularly with the apparent shock not being resolved as sharply.

Figure 4 shows the particle velocities represented as a vector field. A contour line ($\alpha = 0.55$, $t = 6$) is superimposed to show the bubble location more clearly. It is shown in this figure that, located behind the bubble, is a set of counter-rotating convective rolls and these elongate with the passage of time. Figure 5 shows the same contour lines as in Figure 2(c) but this time the streamlines corresponding to the total volumetric flux are superimposed.

5. CONCLUDING REMARKS

The numerical method proposed in this paper is second-order in space. It also has second-order-accuracy in time and is explicit in time. The method captures sharp gradients without the use of a numerical diffusion. The improved accuracy of the second-order method over the first-order method, which is based on simple upwind differencing, is seen from a comparison of the results. The second-order method produces the kidney-shaped bubbles in accordance with physical observations whereas, on the same grid, the first-order method does not. It would require a finer mesh and a much more expensive calculation than that of the second-order method to achieve comparable accuracy when using the first-order method.

A centrally-located jet of a specific width and fluidizing particles of a specific size and density was used to test the numerical method, but it would be worthwhile to adjust the parameters and compare with the wide variety of observed behaviour of jets. Another problem worth considering is a number of much smaller jets dispersed along the length of the distributor to model pores in the material from which the distributor is made. Such studies would allow the consideration of how bubbles are formed as well as how they interact in the bed. In addition, the new information about the dynamics of the bed received from these

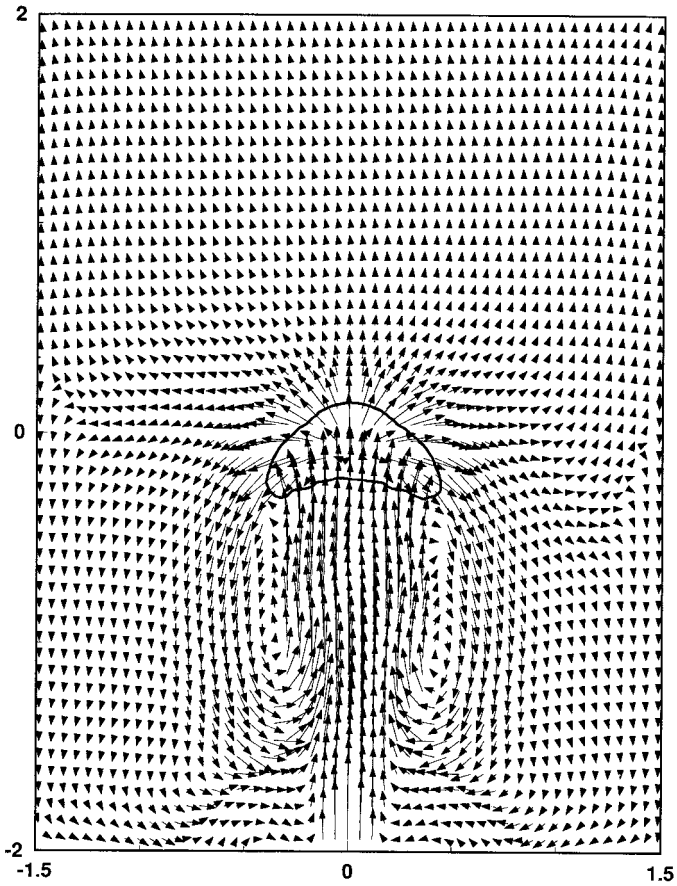

Figure 4. Particle velocity vectors at $t = 6$ with a contour outline of the bubble.

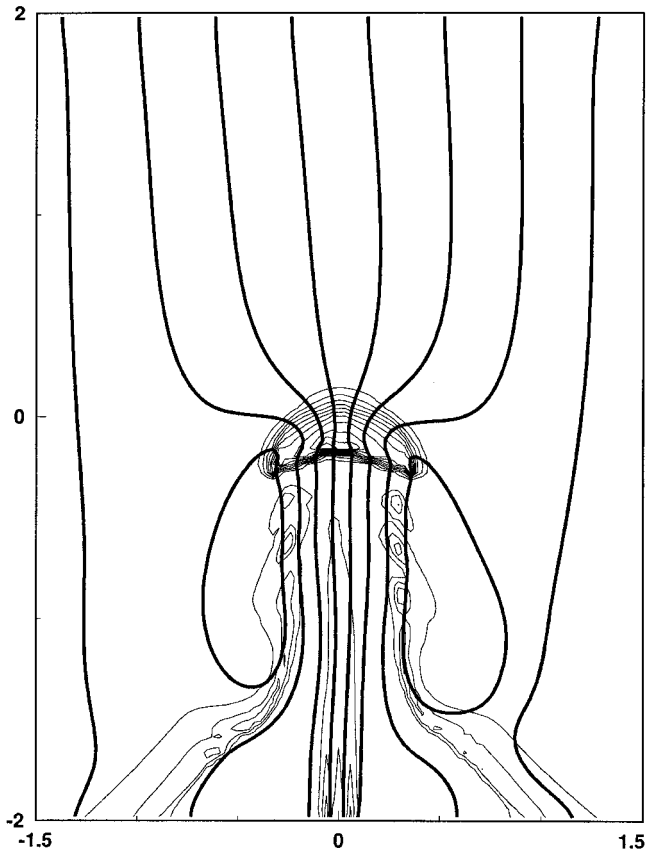

Figure 5. Figure 2(c) with streamlines superimposed.

calculations (namely the existence of a set of convective rolls behind the bubble) may allow new advances in more analytic calculations concerning bubble dynamics.

ACKNOWLEDGMENTS

I. Christie and G.H. Ganser were partly supported by the US Department of Energy, Project DE-FG05-88ER25067. I. Christie was partly supported by the Dirección General de Investigación Científica y Técnica of Spain. J.W. Wilder was partly supported by the National Science Foundation, grant number RII-8922106.

REFERENCES

1. D.A. Drew, 'Mathematical modeling of two-phase flow', *Ann. Rev. Fluid. Mech.*, **15**, 261–291 (1983).
2. A.D. Fitt, 'The character of two-phase gas/particulate flow equations', *Appl. Math. Model.*, **17**, 338–354 (1993).
3. J.B. Fanucci, N. Ness and R.-H. Yen, 'Structure of shock waves in gas-particulate fluidized beds', *Phys. Fluids*, **24**, 1944–1954 (1981).
4. D.J. Needham and J.H. Merkin, 'The propagation of voidage disturbances in a uniformly fluidized bed', *J. Fluid Mech.*, **131**, 427–454 (1983).
5. G.H. Ganser and J. Lightbourne, 'Oscillatory travelling waves in a hyperbolic model of a fluidized bed', *Chem. Eng. Sci.*, **46**, 1339–1347 (1991).

6. I. Christie, G.H. Ganser and J.M. Sanz-Serna, 'Numerical solution of a hyperbolic system of conservation laws with source term arising in a fluidized bed model', *J. Comput. Phys.*, **93**, 297–311 (1991).
7. W.G. Strang, 'On the construction and comparison of difference schemes', *SIAM J. Numer. Anal.*, **5**, 506–517 (1968).
8. P.L. Roe, 'Approximate Riemann solvers, parameter vectors, and difference schemes', *J. Comput. Phys.*, **43**, 357–372 (1981).
9. A. Harten and J.M. Hyman, 'Self adjusting grid methods for one-dimensional hyperbolic conservation laws', *J. Comput. Phys.*, **50**, 235–269 (1983).
10. I. Christie and C. Palencia, 'An exact Riemann solver for a fluidized bed model', *IMA J. Numer. Anal.*, **11**, 493–508 (1991).
11. J.W. Pritchett, T.R. Blake and S.K. Garg, 'A numerical model of gas fluidized beds', *AIChE Symposium Series on Fluidization: Application to Coal Conversion Processes*, **74**, 134–148 (1978).
12. M. Syamlal, 'NIMPF: A computer code for nonisothermal multiparticle fluidization', *EG&G Internal Report*, (1987).
13. M. Syamlal and T.J. O'Brien, 'Computer simulation of bubbles in a fluidized bed', *AIChE Symposium Series on Fluidization and Fluid Particle Systems: Fundamentals and Applications*, **85**, 22–31 (1989).
14. J.B. Fanucci, N. Ness and R.-H. Yen, 'On the formation of bubbles in gas-particulate fluidized beds', *J. Fluid Mech.*, **94**, 353–367 (1979).
15. J.T.C. Liu, 'Note on a wave-hierarchy interpretation of fluidized bed instabilities', *Proc. Roy. Soc. A.*, **380**, 229–239 (1982).
16. J.T.C. Liu, 'Nonlinear wave disturbances in fluidized beds', *Proc. Roy. Soc. A.*, **389**, 331–347 (1983).
17. G.M. Homsy, M.M. El-Kaissy and D.A. Didwania, 'Instability waves and the origin of bubbles in a fluidized bed—II', *Int. J. Multiphase Flow*, **6**, 305–318 (1980).
18. G.H. Ganser, X. Hu and D. Li, 'Solutions for a 2-dimensional hyperbolic-elliptic coupled system', *SIAM J. Math. Anal.*, **27**, 1024–1037 (1996).
19. P. Glaister, 'An approximate linearised Riemann solver for the three-dimensional Euler equations for real gases using operator splitting', *J. Comput. Phys.*, **77**, 361–383 (1988).
20. A.R. Mitchell and D.F. Griffiths, *The Finite Difference Method in Partial Differential Equations*', Wiley, New York, 1980.
21. P.L. Roe, 'Fluctuations and signals—A framework for numerical evolution problems', in K.W. Morton and M.J. Baines (eds.), *Numerical Methods for Fluid Dynamics*, Academic Press, New York, 1982, pp. 219–257.
22. P.K. Sweby, 'High resolution schemes using flux limiters for hyperbolic conservation laws', *SIAM J. Numer. Anal.*, **21**, 995–1011 (1984).

